Martian dust devils: Laboratory simulations of particle threshold

Ronald Greeley,[1] Matthew R. Balme,[1] James D. Iversen,[2] Stephen Metzger,[3]
Robert Mickelson,[4] Jim Phoreman,[5] and Bruce White[6]

Received 30 September 2002; revised 21 January 2003; accepted 7 February 2003; published 17 May 2003.

[1] An apparatus has been fabricated to simulate terrestrial and Martian dust devils. Comparisons of surface pressure profiles through the vortex core generated in the apparatus with both those in natural dust devils on Earth and those inferred for Mars are similar and are consistent with theoretical Rankine vortex models. Experiments to determine particle threshold under Earth ambient atmospheric pressures show that sand (particles > 60 μm in diameter) threshold is analogous to normal boundary-layer shear, in which the rotating winds of the vortex generate surface shear and hence lift. Lower-pressure experiments down to ~65 mbar follow this trend for sand-sized particles. However, smaller particles (i.e., dust) and all particles at very low pressures (~10–60 mbar) appear to be subjected to an additional lift function interpreted to result from the strong decrease in atmospheric pressure centered beneath the vortex core. Initial results suggest that the wind speeds required for the entrainment of grains ~2 μm in diameter (i.e., Martian dust sizes) are about half those required for entrainment by boundary layer winds on both Earth and Mars. *INDEX TERMS:* 6225 Planetology: Solar System Objects: Mars; 0343 Atmospheric Composition and Structure: Planetary atmospheres (5405, 5407, 5409, 5704, 5705, 5707); 3322 Meteorology and Atmospheric Dynamics: Land/atmosphere interactions; 5415 Planetary Sciences: Erosion and weathering; 3307 Meteorology and Atmospheric Dynamics: Boundary layer processes;
KEYWORDS: Mars, dust devils, particle threshold, laboratory simulation

Citation: Greeley, R., M. R. Balme, J. D. Iversen, S. Metzger, R. Mickelson, J. Phoreman, and B. White, Martian dust devils: Laboratory simulations of particle threshold, *J. Geophys. Res.*, *108*(E5), 5041, doi:10.1029/2002JE001987, 2003.

1. Introduction

[2] Aeolian processes are potentially important in modifying the surface of Mars (reviewed by *Wells and Zimbelman* [1989]; *Greeley et al.* [1992]; *Kahn et al.* [1992]; *Zurek et al.* [1992]; *Martin and Zurek* [1993]; and *McKim* [1995]). Recent results from the Mars Pathfinder (MPF) [*Golombek et al.*, 1997, 1999; *Smith et al.*, 1997; *Greeley et al.*, 1999, 2002], Mars Global Surveyor (MGS), and Mars Odyssey missions confirm the presence of abundant aeolian features, including duneforms seen in Mars Orbiter Camera (MOC) high-resolution images [*Malin et al.*, 1998; *Malin and Edgett*, 1999, 2001; *Edgett and Malin*, 2000a; *Cantor et al.*, 2001]. The morphologies and diverse albedo patterns of these features suggest complex histories which might reflect changes in Mars' climate [*Thomas et al.*, 1999]. Moreover, because airborne dust is both an efficient absorber and scatterer of solar radiation, it could strongly influence the thermal structure of the atmosphere [*Kahn et al.*, 1992].

[3] Lander data from Viking and MPF also demonstrate aeolian activity. For example, at the MPF site dust devils were observed in images [*Smith and Lemmon*, 1998; *Metzger et al.*, 1999] and detected in meteorology measurements [*Schofield et al.*, 1997]. Wind-eroded rocks (ventifacts) [*Bridges et al.*, 1999], drifts, and duneforms were also identified, and are considered to reflect the action of wind-blown sand [*Greeley et al.*, 1999, 2002]. Analysis of the orientations of these features and comparisons with features seen from orbit suggest a change in the wind regime through time [*Bridges et al.*, 1998; *Kuzmin and Greeley*, 1999; *Greeley et al.*, 1999].

[4] The observations of dust storms, dust devils, dunes, and other aeolian features on Mars suggest that the transport of sand and dust is important at all scales. The size of dust entrained in the atmosphere is estimated to be only a few microns in diameter [*Pollack et al.*, 1979, 1995; *Smith et al.*, 1997; *Tomasko et al.*, 1999] yet particles this small are very difficult to move by simple boundary-layer wind shear [*Greeley et al.*, 1981; *Iversen and White*, 1982], requiring winds an order of magnitude greater than those measured on the surface of Mars. For this reason, dust devils were proposed to be an efficient mechanism for raising dust [*Neubauer*, 1966; *Sagan and Pollack*, 1969].

[5] In this paper, we briefly review the characteristics of terrestrial and Martian dust devils, describe an apparatus to simulate dust devils, and give initial results from the

[1]Department of Geological Sciences, Arizona State University, Tempe, Arizona, USA.
[2]Aerospace Engineering and Engineering Mechanics Department, Iowa State University, Ames, Iowa, USA.
[3]Department of Geological Sciences, University of Nevada at Reno, Reno, Nevada, USA.
[4]Phoenix, Arizona, USA.
[5]NASA Ames Research Center, Moffett Field, California, USA.
[6]Department of Mechanical and Aerospace Engineering, University of California at Davis, Davis, California, USA.

0148-0227/03/2002JE001987$09.00

apparatus for the entrainment of sand and dust by vortical motions in the atmosphere.

1.1. Terrestrial Dust Devils

[6] Dust devils have been studied for many years on Earth [*Baddeley*, 1860; *Ives*, 1947; *Brooks*, 1960; *Tanner*, 1963; *Sinclair*, 1966; *Idso*, 1974]. They are vortical columns of air and dust that develop from an unstable, near-surface layer of air resulting from surface heating. As outlined by *Sinclair* [1969, 1973], the structure within dust devils consists of a swirling vortex with vertical upward flow forming the core and lateral inflow of air near the bottom of the vortex. He also observed downward flow in the center of some dust devil cores. The tangential velocity profile of many dust devils approximates a Rankine or Lamb-Oseen vortex model [e.g., *Lugt*, 1983; *Green*, 1995]. In the Rankine model, the tangential velocity of the main core is proportional to the radius (solid body rotation), and the tangential velocity of the outer vortex flow is proportional to the inverse of the radius (irrotational vortex), with a sharp peak at the point of greatest tangential velocity. The more complicated Lamb-Oseen model takes into account the frictional loss of angular momentum near the surface and therefore does not contain the unrealistically sharp maximum velocity peak. *Tratt et al.* [2001], however, studied active dust devils in Arizona and, while they found some departures from the Rankine model, they agreed that the overall structure can be approximated by this model. Because of the simplicity of the Rankine vortex model compared to the Lamb-Oseen vortex, we have chosen to use this approximation of the pressure and tangential velocity structure in a dust devil.

[7] On calm days on Earth, the vorticity source for dust devils can be the result of convective circulation leading to "auto-initiation" [*Metzger*, 1999]. Dust devils can also form as spin-off eddies from wind gusts [*Hallett and Hoffer*, 1971], especially when gusts move across a topographically irregular surface [*Metzger and Lancaster*, 1995]. Their formation tends to be suppressed by ambient winds greater than about 8 m/s, depending on the sheltering effects of surface roughness elements [*Sinclair*, 1966; *Ryan and Carroll*, 1970; *Metzger and Lancaster*, 1995]. Once initiated, thermal plumes sustain the vortex. A low-pressure zone in the vortex core draws in additional ground-level air carrying angular momentum. The inward moving mass of rotating air increases in tangential velocity by quasi-conservation of angular momentum; in this region (outside the core) tangential velocity is inversely proportional to the radial distance from the axis of rotation. Inside the core the rotation is approximately solid-body. The vortex commonly develops wind velocities whose surface shear stresses far exceed those of horizontal turbulent winds. This often results in particle saltation which forms a "skirt" of wind-blown sand and dust at the base of the vortex, initiating the entrainment of particles from surfaces otherwise resistant to turbulent wind shear [*Gillette et al.*, 1980].

[8] Once formed, terrestrial dust devils can extend to heights of several kilometers, enabling particles to be carried aloft and transported great distances [*Ives*, 1947; *Hess and Spillane*, 1990]. Dust devils typically have radii of ~1 to 150 m [*Sinclair*, 1966; *Schwiesow and Cupp*, 1975; *Hess and Spillane*, 1990; *Metzger*, 1999] and display maximum tangential velocities of 25 m/s [*Sinclair*, 1966; *Kaimal and Businger*, 1970; *Fitzjarrald*, 1973; *Schwiesow and Cupp*, 1975; *Hess and Spillane*, 1990; *Metzger*, 1999]. The decrease in pressure at the center of dust devils can range from 250 to >2000 Pa [*Sinclair*, 1966; *Metzger*, 1999]. This suggests that the pressure excursion is about 0.25–2% of the ambient pressure, which could enhance the "lift" of fine-grained materials from the surface.

[9] Field studies indicate that terrestrial dust devils can form on a variety of surface roughnesses, including smooth playas and rocky alluvial fans [*Metzger*, 1999]. In addition, local topography can influence dust devil evolution. For example, some dust devils observed in southern Arizona dispersed upon passage over arroyos and channel-like depressions. Recent remote sensing observations of terrestrial dust devil tracks [*Rossi*, 2002] also suggest that local topography can influence their pathways. Although dust devils are local phenomena, their high frequency in some areas suggests that their role in the evolution of dust storms could be significant. For example, *Metzger* [1999] estimates that a single large terrestrial dust devil can inject ~2000 kg of dust into the atmosphere.

1.2. Martian Dust Devils

[10] Dust devils were suggested on Mars [*Neubauer*, 1966; *Sagan and Pollack*, 1969; *Sagan et al.*, 1971; *Ryan and Luchich*, 1983] and then confirmed by *Thomas and Gierasch* [1985], who discovered ~100 dust devils in Viking Orbiter images. These features were as large as 1 km across and extended a few kilometers above the surface (e.g., Figure 1). More recently, *Edgett and Malin* [2000b] found numerous dust devils, some as high as 6 km, in an area of only ~60 km^2. Similarly, *Biener et al.* [2002] identified dust devils as wide as several kilometers on MOC images. Dust devils on Mars are thought to form in a similar manner to those on Earth [*Renno et al.*, 2000].

[11] Active dust devils (~20 m across) observed in MOC images [*Edgett and Malin*, 2000b] left dark tracks (Figure 1b), confirming earlier speculation based on Viking images that some dark streaks on Mars result from the passage of vortices [*Grant and Schultz*, 1987]. Tracks vary from relatively straight, to curvilinear, to looping and "curlicue" patterns. Many of these tracks are only 10s of meters across, although some are 250 m wide. As outlined by *Edgett and Malin* [2000b], the patterns seem to form independently of the terrain over which they pass, including craters, cratered terrain, and fields of sand dunes. Although this is in contradiction to some observations of terrestrial dust devil tracks [*Rossi*, 2002], the lack of remote sensing data of dust devil tracks on Earth make comparison difficult. From various cross-cutting relations, the inferred dark, Martian dust devil tracks appear to become brighter with time. This is considered to result from an initial formation in which bright dust is removed from the surface beneath the vortex core, exposing a darker substrate. With time and as dust settles from the atmosphere, the track becomes mantled and hence brighter.

[12] Dust devils have also been detected from landers on Mars and analyzed [*Ringrose and Zarnecki*, 2002]. For example, the MPF meteorology data suggest that numerous atmospheric vortices passed over the lander [*Schofield*

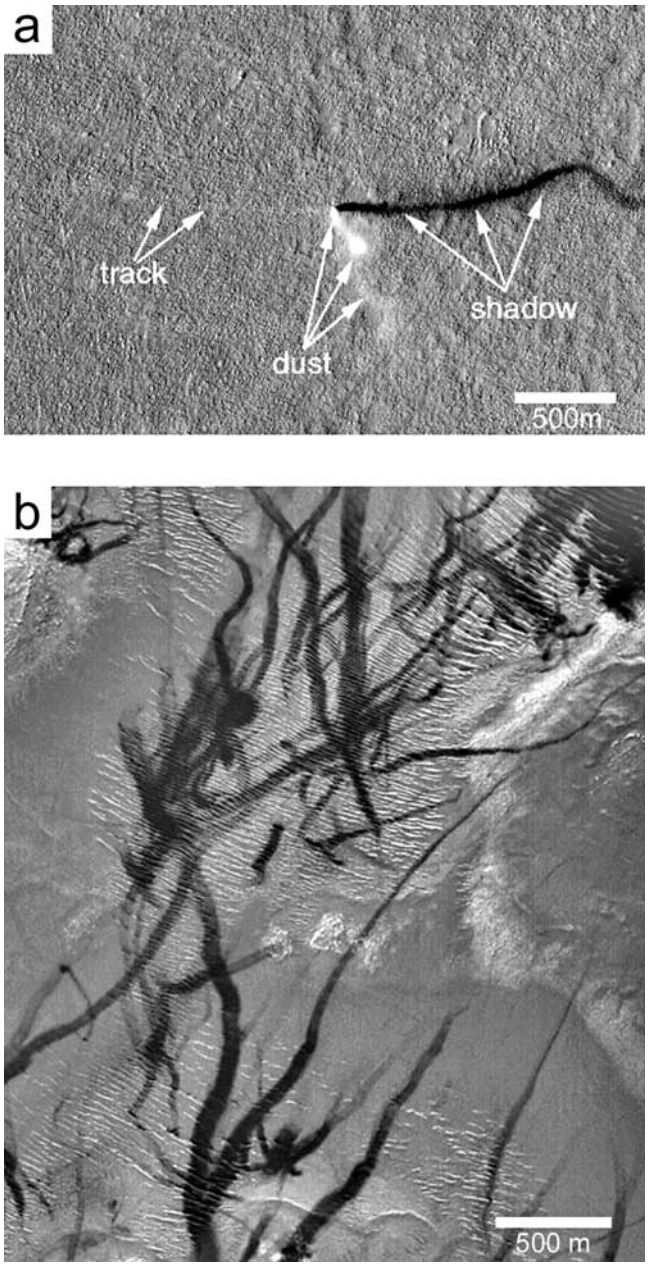

Figure 1. (a) This active dust devil was imaged by the Mars Observer Camera; the shadow cast by the dust lifted from the surface indicates the relatively uniform diameter of the vortex core (NASA image PIA 03223) from Malin Space Science Systems. (b) These dark streaks are considered to be tracks on the surface left by the passage of active dust devils (NASA image PIA 02376, Malin Space Science Systems).

et al., 1997], from which pressure excursions of 1–5 Pa were measured (at a height ~10 cm above the Mars surface [*Seiff et al.*, 1997]) equating to ~0.2–1.0% of ambient pressure. In addition, the MPF camera captured at least five dust devils which developed in rapid succession [*Smith and Lemmon*, 1999; *Metzger et al.*, 1998a, 1998b, 2000]. These results occurred during a relatively calm period on Mars (L_s = 143°), when maximum surface winds were no more than about ~10 m/s (*Schofield et al.*, 1997), far less than boundary-layer threshold for the movement of sand and dust, and strongly suggesting that dust devils are an effective mechanism for particle entrainment [*Metzger*, 2001].

[13] Wind speeds measured by the Viking landers and MPF never reached sufficient values to entrain the fine dust seen in the atmosphere. Consequently, numerous other mechanisms have been proposed to raise dust on Mars (reviewed by *Greeley et al.* [1992]), including: 1) dust fountaining by gas desorbtion, 2) impact by sand saltation to "kick up" dust, 3) aggregation of particles to form "clumps" that are more easily moved, and 4) entrainment by dust devils. The dust devil hypothesis is attractive, particularly given their apparent high frequency on Mars [*Thomas and Gierasch*, 1985; *Edgett and Malin*, 2000b; *Beiner et al.*, 2002]. Yet, despite the potential importance of dust devils in understanding the aeolian regime on Mars, little is known about their mechanisms for setting dust into motion.

2. Approach

[14] Planetary research often requires a multipronged approach, including numerical modeling, laboratory simulations, and field studies. Each technique has unique attributes: field investigations involve full-scale events, but the complexities of natural processes often do not enable isolation of the critical variables for analysis. Moreover, the influence of some parameters for application to Mars, such as the low atmospheric density, cannot be assessed in field work on Earth. Numerical and analytical studies enable some of these variables to be assessed, but computer models are often over simplified. Laboratory simulations, the primary approach used here, have the advantage that experiments can be run under controlled conditions in which critical variables can be isolated for analysis, and in which certain environmental conditions can be simulated for Mars, such as the low atmospheric surface pressure. Finally, it should be stressed that our methodology focuses on how dust devils entrain material on Earth and Mars rather than how dust devils are formed.

2.1. ASU Vortex Generator

[15] The Arizona State University Vortex Generator (ASUVG) [*Greeley et al.*, 2001; *Balme et al.*, 2001, 2002] was fabricated to simulate dust devils in the laboratory. It consists of three components, the frame, the vortex generator, and the test table (Figure 2). The apparatus can be dismantled for transport into the field for conducting experiments on natural surfaces and for use in a low-pressure chamber at NASA Ames Research Center for tests under Martian atmospheric conditions. The vortex generator includes a cylinder (45 cm in diameter by 1.3 m long) with a "bell mouth" to alleviate boundary effects at the edge of the cylinder, a motor drive, and a fan blade system. The generator is mounted to the frame so that it can be lowered or raised above the test table, enabling the geometry of the simulated dust devil to be varied. The table is 2.4 by 2.4 m, mounted independent of the frame which holds the vortex generator so that potential motor vibrations are isolated from the test bed. The table can be raised or lowered,

Figure 2. The Arizona State University Vortex Generator (ASUVG) includes the vortex tube which contains the vortex blades and motor isolated beneath the vortex tube is the test bed, which is instrumented with pressure transducers. In this photograph, the vortex is visible using ablation of dry ice.

moved laterally to simulate motion of a dust devil across terrain features, and tilted to simulate a vortex that is not perpendicular to the surface.

[16] The ASUVG is instrumented to measure the ambient temperature and relative humidity, and wind speeds and surface pressures on the test bed beneath the vortex. Pressures are measured continuously from 14 stations (flush-mounted pressure transducers manufactured by Setra), which can be placed in a variety of configurations. All data are processed by Labview software.

[17] More than 1000 runs have been made to calibrate vortex generator speeds (RPM), pressure profiles, and geometric configurations of the vortex as functions of cylinder heights above the table. Of particular importance is the distribution of atmospheric pressure through the vortex core, because comparisons can be made with natural, full-scale dust devils on Earth and Mars for which similar measurements have been made.

[18] The structure of a dust devil at the surface, whether real or simulated in the laboratory, is characterized by a decrease in pressure (ΔP) at the center of the vortex with regard to the static pressure and by the vortex core radius (r_o), which can be derived from pressure profiles taken at the surface. In our experiments we have found that the value of ΔP at the center of the vortices is proportional to the square of the rotational velocity of the vortex generator but independent of the core radius, consistent with the body of the vortex being in cyclostrophic equilibrium (i.e., the pressure gradient force on a unit mass of air is equal in magnitude to the centripetal acceleration of the mass and so particles move in circular orbits with no radial velocity) such that

$$\frac{v_o^2}{r} = \frac{1}{\rho}\frac{\partial P}{\partial r} \tag{1}$$

in which v_o is the tangential flow velocity, r is the distance from the center of revolution, ρ is the density of the air (assumed constant over the flow as the small deviations in pressure do not significantly effect the density), P is the pressure and $\partial P/\partial r$ is the pressure gradient at the distance r. The vortex core radius, r_o, is defined as the distance from the center of the vortex to the point at which the product $r\partial P/\partial r$ (an approximation of the square of the tangential velocity, v_t, in the flow) is a maximum. The maximum tangential velocity also occurs at this radius if the more complicated Lamb-Oseen vortex model is used. We use plots of $r\partial P/\partial r$ against r to extract r_o and $v_{t(max)}$ as a function of apparatus geometry, generator speeds and ambient pressure. Figure 3 shows an example of a plot with the values of r_o and $v_{t(max)}$ identified. In addition, observations using ablation of dry ice for flow visualization show that the core radius is constant throughout the height of the vortex and that, similar to full-scale dust devils, most of the inflow is at the surface of the test bed. We also observe a qualitative similarity between laboratory vortices and natural dust devils (Figure 4) when sand and dust is placed on the test bed: the core and upper part of the vortex is composed of fine dust, whereas a "skirt" of larger particles surrounds the base.

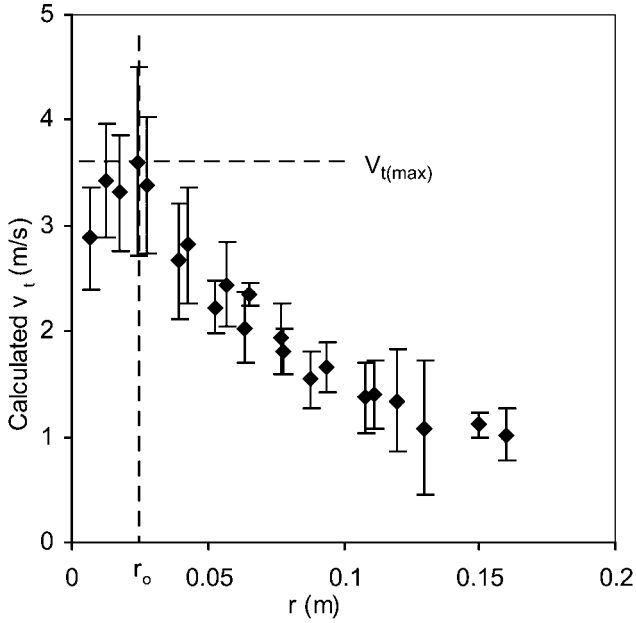

Figure 3. Typical plot of calculated v_t ($v_t^2 = r/\rho.\partial P/\partial r$) as a function of distance from the center of revolution in the vortex. These plots allow an estimate of the highest tangential velocity in the flow, $V_{t(max)}$, and the radius of the vortex core, r_o. Error bars reflect standard deviation of the measurement of pressure gradient.

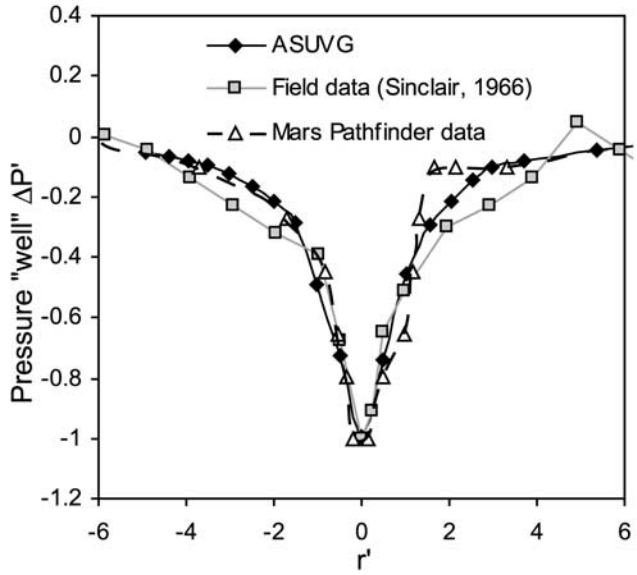

Figure 5. Dimensionless pressure profile for Earth, Mars, and laboratory-scale vortices; $r' = 0$ is the approximate center of the vortex core. The profiles are scaled using nondimensional parameters $\Delta P'$ and r' in which $\Delta P' = 1$ is defined as the depth of the pressure well and $r' = 1$ is defined as the radius at which the pressure deficit is one half of the total ΔP.

[19] Experiments at Mars equivalent pressure (i.e., 10 mbar air at Earth ambient temperature has the same fluid density as ~6 mbar CO_2 at Mars mean surface temperature) using high vortex generator speeds show similitude with one bar (i.e., "Earth") experiments running at lower speeds and the pressure profiles are very similar in shape to full-scale dust devils on Earth and Mars (Figure 5). In addition to the dependence of ΔP on the square of generator speed, the calculated peak tangential velocity $v_{t(max)}$ is directly proportional to the vortex generator speed.

[20] The change in ΔP and $v_{t(max)}$ with decreasing ambient pressure is nonlinear; below 100 mbar the vortex generator must be run at increasingly higher speeds to generate the same values of ΔP or $v_{t(max)}$. Vortex core radii observed at low atmospheric pressures are very similar to those observed at one atmosphere, indicating that, for fixed apparatus geometry, the vortex core radius is a constant but ΔP depends upon both atmospheric pressure and vortex generator rotational velocity.

[21] On the basis of the similarity of ASUVG vortices and natural dust devils (Figure 4), the similitude of the ΔP

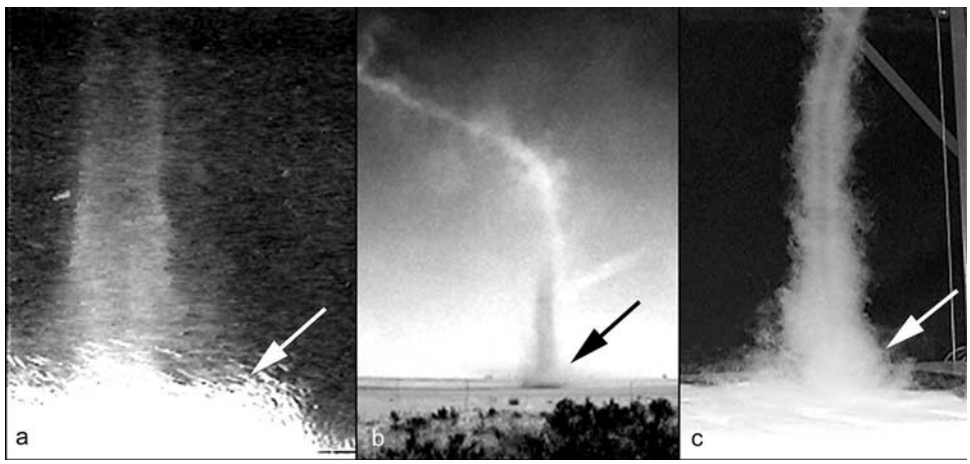

Figure 4. Comparison of a) particle entraining laboratory vortex simulation; b) terrestrial dust devil; c) laboratory vortex using sublimation of dry ice for visualization. Note the clear core with constant radius in "c" and the well-defined dust- loaded core in the laboratory image "a" and the similar structure in the natural dust devil. The "saltation skirt" zone is indicated by an arrow in each case.

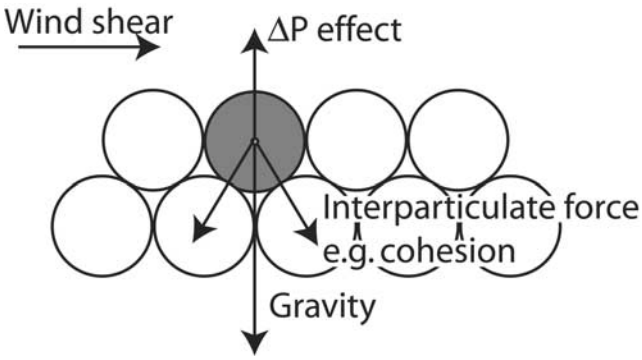

Figure 6. Forces on a particle at the point of movement beneath an atmospheric vortex.

(Figure 5), and the calibrations of the vortex speeds, we were able to initiate experiments to determine particle threshold by vortices.

3. Particle Threshold by Vortices

[22] Relatively few measurements of particle threshold have been made in field studies of dust devils [*Metzger*, 1999] or previous laboratory simulations [*Hsu and Fattahi*, 1976]. Although limited, results from these measurements show that vortex motions can lift both sand and dust, and that vortex motion appears to be more efficient than simple boundary layer winds for lifting dust [*Greeley et al.*, 1977; *Greeley and Iversen*, 1985].

[23] There are at least two mechanisms by which dust devils lift particles into the atmosphere. The first is the upward component of force caused by frictional drag of winds moving over the bed of particles, which is analogous to the wind shear that lifts particles in simple boundary layer winds [*Bagnold*, 1941]. The second mechanism, which we refer to as the "ΔP effect" is the decrease in pressure found at the center of dust devils (Figure 5) which leads to a lift on the particles as the vortex sweeps across the surface. Opposing these effects are the weight of the particles and inter-particle cohesion (Figure 6).

[24] The lifting effect of the wind shear is relatively easy to derive if the velocity of the vortex is known, as it depends on the greatest wind velocity in the flow. This effect has been studied extensively in boundary layer wind tunnels for both Earth and Mars conditions [e.g., *Iversen et al.*, 1973; *Greeley et al.*, 1977, 1981]. The lifting effect of the pressure decrease at the surface is less easy to quantify because it depends on unknown factors such as how deeply the ΔP effect propagates into the bed of particles and how quickly the pressure deficit is applied.

[25] Our measurements of ΔP as a function of vortex speed, vortex diameter, and atmospheric pressure quantify the ΔP lift available for threshold. These "calibration" measurements can then be applied to the threshold experi-

Table 1. Threshold Test Matrix[a]

			"Earth" Case	Atmospheric Pressure																								"Mars" Case		
			1021 mbar	655 mbar			440 mbar			187 mbar			95 mbar			67 mbar			40 mbar			27 mbar			15 mbar			10 mbar		
Particle Type	Particle Size, μm	Particle Density, g/cm^3	1	2	3	1	2	3	1	2	3	1	2	3	1	2	3	1	2	3	1	2	3	1	2	3	1	2	3	1	2	3
Walnut shells	212	1.3	X	X	X		X		X	X	X		X			X			X			X		X	X	X		X			X	
Walnut shells	311	1.3	X	X	X		X						X			X						X			X			X			X	
Walnut shells	393	1.3	X	X	X																											
Walnut shells	527	1.3	X	X	X																											
Walnut shells	660	1.3	X	X	X																											
Walnut shells	880	1.3	X	X	X	X	X	X	X	X	X	X	X	X	X	X	X	X	X		X				X	X				X	X	
Walnut shells	1097	1.3	X	X	X																											
Walnut shells	1299	1.3	X	X	X																											
Walnut shells	1862	1.3	X	X	X		X		X	X	X		X			X			X		X	X	X		X			X				
Silica sand	212	2.7	X	X	X																											
Silica sand	311	2.7	X	X	X																											
Silica sand	393	2.7	X	X	X	X	X	X	X	X	X	X	X	X	X	X	X	X	X	X	X	X	X	X	X	X		X	X	X	X	
Silica sand	527	2.7	X	X	X																											
Silica sand	660	2.7	X	X	X																											
Chromite	230	4.8	X	X	X	X	X	X	X	X	X	X	X	X	X	X	X	X	X	X	X	X	X	X	X	X	X	X	X	X	X	X
Alum. oxide	311	3.8	X	X	X	X	X	X	X	X	X	X	X	X	X	X	X	X	X	X	X	X	X	X	X	X	X	X	X	X	X	X
Alum. oxide	527	3.8	X	X	X																											
Alum. oxide	660	3.8	X	X	X																											
Alum. oxide	1097	3.8	X	X	X																											
Alum. oxide	1299	3.8	X	X	X																											
Steel grit	212	7.6	X	X	X																											
Steel grit	311	7.6	X	X	X																											
Steel grit	768	7.6	X	X	X		X			X			X			X																
Steel grit	1097	7.6	X	X	X		X			X	X		X			X																
Silica flour	8	2.5	X	X	X				X	X	X	X	X	X	X	X	X	X	X	X	X	X	X	X	X	X	X	X	X	X	X	X
Silica beads	35	2.5	X	X	X					X			X			X	X		X		X	X	X	X	X	X				X	X	X
Silica beads	42	2.5	X	X	X				X	X	X	X	X	X	X	X	X	X	X	X	X	X	X	X	X	X				X	X	X
Silica beads	59	2.5	X	X	X																											
Silica beads	86	2.5	X	X	X				X	X	X	X	X	X	X	X	X	X	X	X	X	X	X	X	X	X	X		X	X	X	X
Carb. R. clay	2	2.6	X	X	X								X			X			X			X	X	X		X	X			X	X

[a]"X" represents a completed threshold test. The header of each column describes the pressure and the vortex radius (1 = 7.5 cm, 2 = 3.5 cm, 3 = 2 cm) at which the tests were performed.

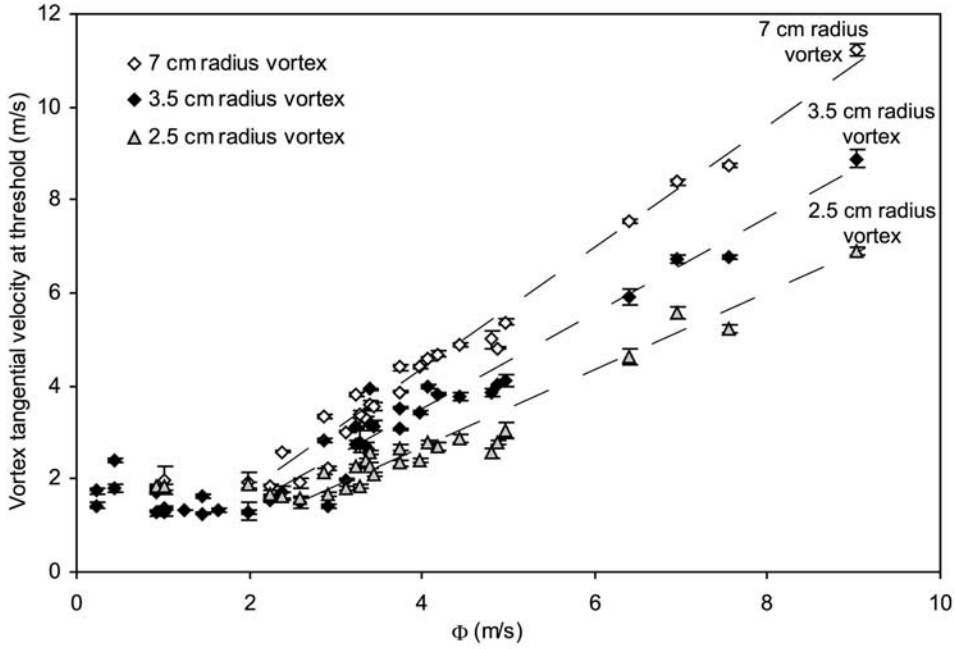

Figure 7. Earth ambient pressure vortex threshold results for all materials as a function of the threshold parameter, Φ. The threshold values are approximately linear with increasing particle size for sands and there are differences in this region among the data for different vortex core radii. The data become more compressed for the smaller particles and there is an increase in the maximum tangential velocity required for threshold.

ments in order to assess the importance of ΔP versus wind shear as functions of particle density, particle diameter, atmospheric pressure, and surface roughness.

[26] We build on the results of *Greeley et al.* [1981] and *Greeley and Iversen* [1985] who first attempted to understand the threshold of particles subjected to vortices. They considered the force balance of a particle at the point of vortex threshold:

$$k_1\Delta P + k_2\tau = k_3\rho_p g D_p + k_4\sigma_p \quad (2)$$

in which τ is the shear stress caused by the swirling wind, ρ_p is the density of the particles, g is gravity, D_p is the particle diameter, and σ_p the inter-particle cohesive stress. k_{1-4} are constants indicating the relative importance of the stresses. Our threshold experiments were run to quantify k_{1-4} using various particle densities and diameters (Table 1). For each material, three types of threshold were recorded (first movement, intermittent saltation, and continuous saltation; continuous saltation is the result used here). Particle threshold was detected using a television camera viewing the test bed illuminated by a collimated 1000 W light beam oriented perpendicular to the camera. This enabled the moving particles to be visible as "fireflies" (bright spots) against a dark background, which provided reasonably consistent measurements of threshold.

[27] Test materials included walnut shells (ρ_p, 1300 kgm^{-3}), silica (ρ_p, 2500–2700 kgm^{-3}), aluminum oxide (ρ_p, 3800 kgm^{-3}), chromite (ρ_p, 4800 kgm^{-3}), steel grit (ρ_p, 7600 kgm^{-3}) and Carbondale Red Clay (ρ_p, 2600 kgm^{-3}). These particle densities follow a parametric hierarchy and enable an approximation of the difference in gravity

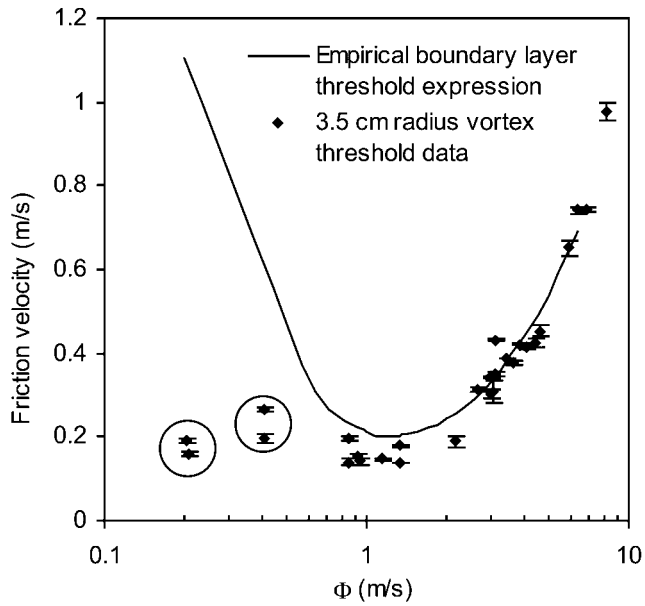

Figure 8. Earth ambient pressure threshold results for 3.5 cm radius vortex core for all materials with a density >2000 kgm^{-3} as a function of the threshold parameter, Φ plotted against the empirical boundary layer threshold expression from *Iversen et al.* [1976a, 1976b], *Greeley and Iversen* [1985], and *Iversen et al.* [1987]. The data with the lowest value of Φ (circled) are for the smallest particles (2 μm Carbondale Red Clay and 8 μm silica flour) and plot below the boundary layer threshold expression.

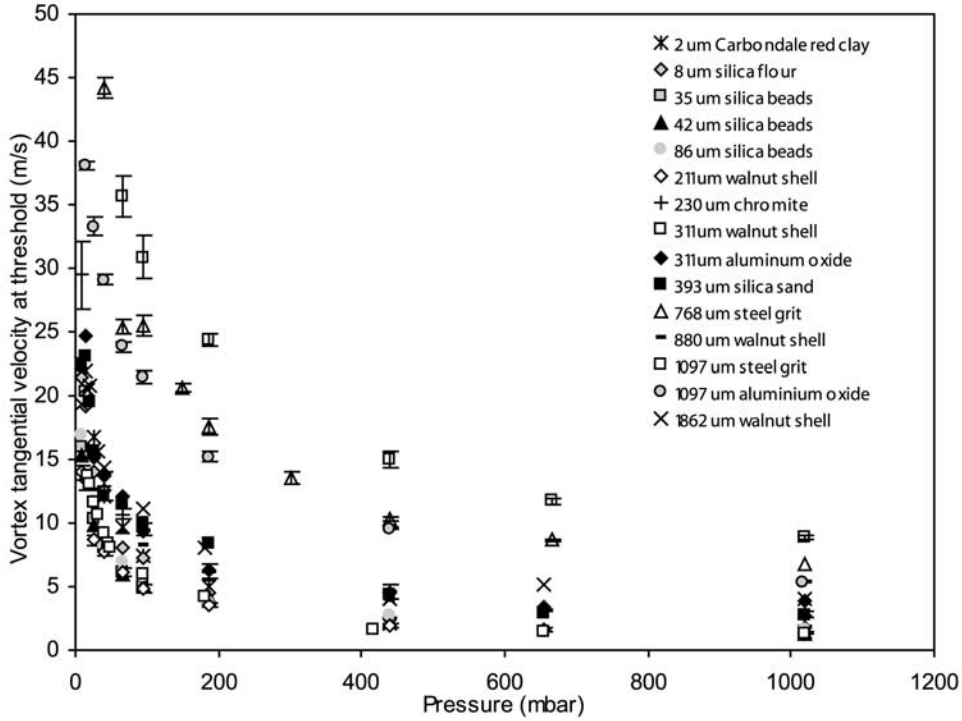

Figure 9. Vortex threshold test results for 3.5 cm core radius vortex as a function of atmospheric pressure. Error bars represent measurement uncertainty and are marked only for the larger, denser particles. Error bars for the other data are omitted in the sake of clarity but are typically <5% of the threshold value with the lowest pressure data having uncertainties up to ~8%.

between Earth and Mars (i.e., for lift-off during particle threshold, the walnut shells are of lower density, and hence "easier" to lift due to less weight, as would be the case in the lower gravity on Mars). Particle sizes ranged from 2 to 1850 microns in diameter, similar to those used in previous threshold tests under simple boundary-layer conditions [e.g., *Iversen et al.*, 1976a, 1976b; *Greeley et al.*, 1977, 1981; *Iversen and White*, 1982] and enabled comparisons with the previous experiments. Particles <70 μm in size were aerodynamically settled onto the test bed to form a layer ~1 mm thick. The method used to emplace such air fall beds is similar to that of *White et al.* [1997] and *Greeley et al.* [2000] and uses a small bucket of test material mixed with sand. The bucket has a compressed air input near the base and a screen over the opening with mesh size too small for the sand to pass through. The whole apparatus is positioned within a "tent" to contain the dust. When compressed air is injected, the sand and dust are agitated and a cloud of dust rises from the bucket to fill the tent and, with time, settles from suspension to form a smooth air fall bed. Beds of larger particles were placed into a circular recess ~1.2 m in diameter and ~1.5 cm depth in the test bed and leveled to form a smooth surface.

3.1. Vortex Threshold at Earth Ambient Pressure

[28] We present results in terms of calculated maximum vortex tangential velocity at threshold and a threshold parameter, Φ, defined as $\sqrt{(\rho_p g D_p)/\rho}$, which allows comparison with boundary layer thresholds [*Iversen et al.*, 1976a, 1976b; *Greeley et al.*, 1977, 1981; *Iversen and White*, 1982]. Results for Earth atmospheric pressure (Figure 7) show a linear trend between threshold velocity and Φ for sand-size particles (particle size > 60 μm and therefore Φ greater than ~1.5 m/s), and an increase in velocity for smaller particles, similar to the relation seen for simple boundary layer conditions. The results from three experiments with different vortex core radii (achieved using different geometries of the ASUVG; the higher the cylinder above the test bed, the narrower the vortex formed) each showed linear trends between threshold velocity and Φ but with different slopes. This result is inconsistent with ΔP lift being a dominant mechanism for particles > 60 μm diameter because ΔP in our calibration experiments was independent of vortex radius. Thus we infer that wind shear in the vortex is the dominant mechanism for sand sized particles at one atmosphere pressure; therefore $k_1 \ll k_2$ and $k_4 \ll k_3$ (because the magnitude of the interparticle cohesion is much less than the weight of sand sized particles) and in this case, from equation (2),

$$k_2\tau = k_3\rho_p g D_p \tag{3}$$

which is directly analogous to simple boundary-layer threshold.

[29] In simple boundary-layer threshold theory

$$\tau = A^2\rho_p g D_p \tag{4}$$

in which A is Bagnold's coefficient, which can be approximated as 0.11 for sand size particles at Earth pressure [*Iversen et al.*, 1976a]. However, for small particles, A is not

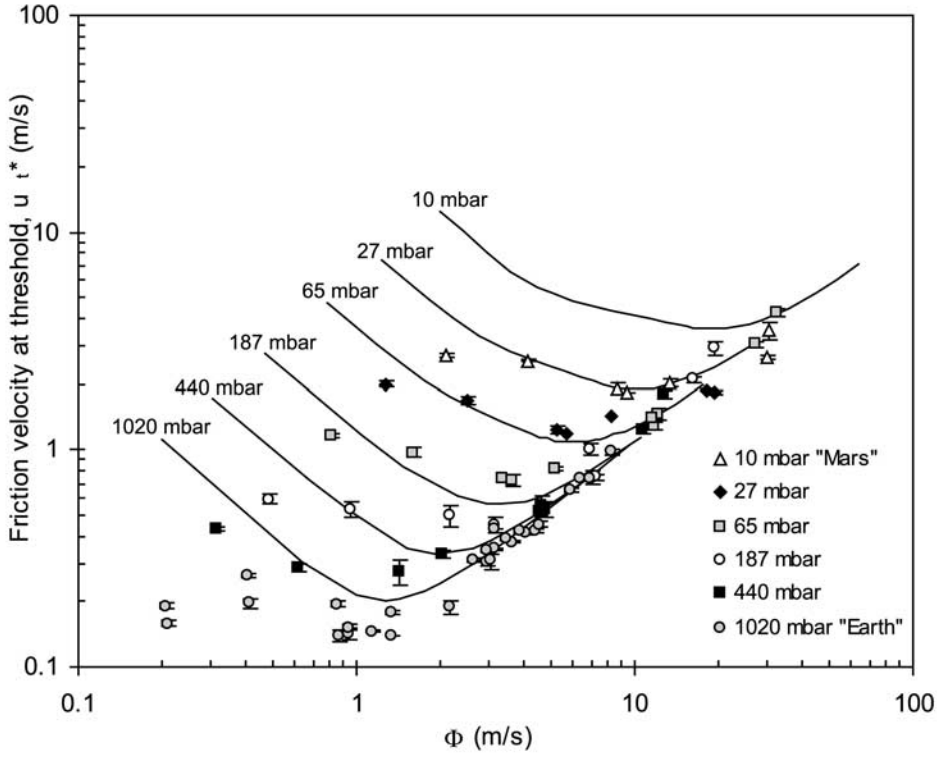

Figure 10. Low-pressure vortex threshold test results for particle with densities >2000 kgm^{-3} with a 3.5 cm core radius vortex as a function of threshold parameter, Φ. Each set of data is compared to an empirically derived normal boundary layer threshold expression, corrected for particle size and particle friction Reynolds number. The vortex threshold data are scaled to fit the boundary layer data in the linear region using the factor 0.12. Error bars are derived from initial determination of vortex generator RPM at threshold.

fixed because it is a function of particle size (due to increasing cohesion for progressively smaller particles) and particle friction Reynolds number, B, defined as

$$B = u_* D_p/\nu \tag{5}$$

where u_* is the friction velocity (defined as $u_* = \sqrt{\tau/\rho}$) and ν is the kinematic viscosity of the atmosphere. Thus the simple approximation for A can only be extended to dust-size particles and different atmospheric conditions if normalized for D_P and B. Such an empirical expression for A has been derived from extensive boundary-layer experiments [*Iversen et al.*, 1976a, 1976b; *Greeley et al.*, 1977, 1981; *Iversen and White*, 1982] which resulted in the equations

$$A = 0.266\left(\frac{1 + 5.5 \times 10^{-5}/\rho_p g D_p^2}{1 + 2.123B}\right)^{1/2} \qquad B \le 0.22 \tag{6a}$$

$$A = \left(0.108 + 0.0323/B - 0.00173/B^2\right) \cdot\left(1 + 5.5 \times 10^{-5}/\rho_p g D_p^2\right)^{1/2} \qquad 0.22 \le B \le 10 \tag{6b}$$

$$A = 0.11 \qquad B \ge 10 \tag{6c}$$

These equations are transcendental in u_* and can be solved iteratively to give an expression for u_* as a function of Φ [*Iversen et al.*, 1976b]. The constants included are dimensionless except for 5.5×10^{-5} which has units kgs^{-2}.

[30] Because interpretation of our data suggest that vortex and boundary layer threshold are equivalent for sand particles, we can plot the vortex data (for a given vortex core radius) over this empirical boundary layer curve (6) by applying a fixed scaling factor to the vortex threshold data to fit the sand-size vortex data to the sand-size boundary-layer expression. Then, if the particle entraining mechanisms of both the vortex and the normal boundary-layer are the same, the curves should be similar for all particle sizes and densities. For example, Figure 8 shows vortex thresholds for all particles with density > 2000 kgm^{-3} (less dense particles diverge from the boundary-layer approximation for the smaller sand particles [*Greeley and Iversen*, 1985, p. 77]) plotted together with the empirical boundary-layer threshold curve (6). Figure 8 shows that, for the smallest values of Φ, the boundary-layer approximation "over corrects" the vortex data. In fact, where the empirical boundary-layer deviates most from the vortex data in Figure 8 (for the smallest particles with the lowest value of Φ) the difference reduces the u_* needed for particle movement by almost 80%. This supports the concept of an additional lifting mechanism in vortex threshold, which we infer to be the additional ΔP effect.

[31] The Earth atmosphere data indicate that threshold for dust is more easily obtained by vortical atmospheric motions than a boundary-layer wind. This has been observed in natural dust devils (i.e., entrainment of dust under relatively calm boundary layer wind flow) but our result is the first time that the process has been quantified.

3.2. Vortex Threshold at Low Pressures

[32] The vortex threshold is plotted as a function of atmospheric pressure in Figure 9. Data indicate a nonlinear relationship in which there is relatively little change in slope between 1000 and 100 mbar with a much larger increase between 100 and 10 mbar. This nonlinear dependence of threshold on pressure suggests that even small increases in atmospheric pressure can substantially facilitate entrainment of particles. This result suggests that dust devils would entrain material more easily in the regions of Mars with greatest surface pressure. Thus we suggest that dust devils might be more common in the lowest regions of Mars, all other factors being equal.

[33] Following the method used for the Earth (one bar) data, we graphed the low-pressure threshold results for particles with $\rho_p > 2000$ kgm^{-3} as a function of Φ for comparisons with boundary-layer threshold. We applied a scaling constant to the tangential velocity at threshold for each value of atmospheric pressure and overlaid the results so that the data for sands fit the boundary-layer expression (Figure 10). The scaling factor used was 0.12; however, it is noted that for pressures <65 mbar there were no data to plot directly onto the linear part of the boundary layer expression.

[34] Consistent with the results of the one-bar experiments, the data for low atmospheric pressure suggest that vortices are more efficient in entraining dust than boundary layer winds. In addition, the vortex threshold data for the Mars case are lower than the boundary layer curve, suggesting that at very low pressure, vortices are far more efficient than boundary layer winds at entraining particles of all sizes. Note, however, that threshold could not be achieved for large, dense particles at the 10 mbar Mars equivalent atmosphere because of insufficient speed by the vortex generator, and the best-fit scaling was extrapolated from the experiments run at higher pressures.

4. Conclusions

[35] The ASU Vortex Generator appears to produce valid simulation of dust devils demonstrated by near-surface pressure profiles that are similar to those for terrestrial dust devils measured in the field and those measured on Mars. Moreover, the calculated tangential velocity structure of the laboratory scale vortices is similar to field measurements and theoretical Rankine vortex models.

[36] Our experiments suggest that vortex threshold is directly analogous to normal boundary layer shear for sand-size particles at Earth (1 bar) pressures. Thus, to understand the sand-lifting power of a dust devil, we need knowledge of the velocity structure within the vortex. In contrast, fine dust is more easily moved by a vortex than when subjected to boundary-layer winds. We suggest that the decrease in atmospheric pressure at the center of the vortex provides an additional lift function. When we extend the experiments to atmospheric pressures as low as 65 mbar, we find similar results to Earth (1 bar) conditions. Although our data also suggest that vortex threshold becomes even more efficient at lower pressure, this assertion is based upon a less rigorous extrapolation of results from the experiments run between 1020 and 65 mbar.

[37] We conclude that for all pressures, the ΔP effect (i.e., the decrease in atmospheric pressure under the vortex cove) is the most likely mechanism for enhanced vortex lift. If our scaling factor of 0.12 is appropriate for the 10 mbar data, we estimate that 2 μm dust at 10 mbar atmospheric pressure will be entrained by a dust devil with tangential wind speeds of around 20–30 m/s. On Mars, this speed would be decreased by the lower gravity and would be substantially less than the boundary layer wind speeds to entrain such particles, which are > 100 m/s [*Greeley et al.*, 1992]. Experiments suggest that the wind speeds necessary for entrainment of very small (~2 μm) particles by Martian dust devils are about 20% of those required for entrainment by boundary-layer winds.

[38] **Acknowledgments.** We thank Gary Beardmore and Diana Branson for assistance in running experiments at Arizona State University, Gabriel Zavala-Diaz for assistance at NASA-Ames, and Stephanie Holaday for aid in preparing the manuscript. We also thank Dallas Kingsbury, Laboratory Manager, ASU Civil and Environmental Engineering, for substantial assistance in writing appropriate code for LabView. This work was supported by the National Aeronautics and Space Administration through the Planetary Geology and Geophysics Program and the Mars Exploration Program.

References

Baddeley, P. F. H., *Whirlwinds and Dust Storms of India*, Bell and Daldey, London, 1860.

Bagnold, R. A., *The Physics of Windblown Sand and Desert Dunes*, Methuen, New York, 1941.

Balme, M. R., R. Greeley, B. Mickelson, J. Iversen, G. Beardmore, and S. Metzger, A laboratory scale vortex generator for simulation of Martian dust devils, *Eos Trans. AGU*, *82*(47), Fall Meet. Suppl., abstract P31A-0542, 2001.

Balme, M. R., R. Greeley, B. Mickelson, J. Iversen, G. Beardmore, and D. Branson, Dust devils on Mars: Results from thresholds tests using a vortex generator, *Lunar Planet. Sci*. [CD-ROM], *XXXIII*, abstract 1048, 2002.

Biener, K. K., P. E. Geissler, A. S. McEwen, and C. Leovy, Observations of dust devils in MOC wide angle camera images, *Lunar Planet. Sci*. [CD-ROM], *XXXIII*, abstract 2004, 2002.

Bridges, N. T., R. Greeley, A. F. C. Haldemann, K. E. Herkenhoff, M. Kraft, T. J. Parker, and A. W. Ward, Orientation of aeolian flutes at the Mars Pathfinder landing site, *Lunar Planet. Sci*. [CD-ROM], *XXIX*, abstract 1530, 1998.

Bridges, N. T., R. Greeley, A. F. C. Haldemann, K. E. Herkenhoff, M. Kraft, T. J. Parker, and A. W. Ward, Ventifacts at the Pathfinder landing site, *J. Geophys. Res.*, *104*(E4), 8595–8615, 1999.

Brooks, H. B., Rotation of dust devils, *J. Meteorol.*, *17*, 84–86, 1960.

Cantor, B. A., P. B. James, M. Caplinger, and M. J. Wolff, Martian dust storms: 1999 Mars Orbiter Camera observations, *J. Geophys. Res.*, *106*, 23,653–23,689, 2001.

Edgett, K. S., and M. C. Malin, New views of Mars eolian activity, materials, and surface properties: Three vignettes from the Mars Global Surveyor Orbiter camera, *J. Geophys. Res.*, *105*, 1623–1650, 2000a.

Edgett, K. S., and M. C. Malin, Martian dust raising and surface albedo controls: Thin, dark (and sometimes bright) streaks and dust devils in MGS high-resolution images, *Lunar Planet. Sci*. [CD-ROM], *XXXIII*, abstract 1073, 2000b.

Fitzjarrald, D. E., A field investigation of dust devils, *J. Appl. Meteorol.*, *12*, 808–813, 1973.

Gillette, D. A., J. Adams, A. Endo, D. Smith, and R. Kihl, Threshold velocities for input of soil particles into the air by desert soils, *J. Geophys. Res.*, *85*, 5621–5630, 1980.

Golombek, M. P., and Mars Pathfinder Team, Overview of the Mars Pathfinder mission: Launch through landing surface operations, data sets and science results, *J. Geophys. Res.*, *104*, 8523–8554, 1999.

Golombek, P. M., et al., Overview of the Mars Pathfinder mission and assessment of landing site predictions, *Science*, *278*, 1743–1748, 1997.

Grant, J. A., and P. A. Schultz, Possible tornado-like tracks on Mars, *Science*, *237*, 883–885, 1987.

Greeley, R., and J. Iversen, *Wind as a Geologic Process on Earth, Mars, Venus and Titan*, Cambridge Univ. Press, New York, 1985.

Greeley, R., B. R. White, J. B. Pollack, J. D. Iversen, and R. N. Leach, Dust storms on Mars: Considerations and simulations, *NASA Tech. Memo.*, *78423*, 1977.

Greeley, R., B. R. White, J. B. Pollack, J. D. Iversen, and R. N. Leach, Dust storms on Mars: Considerations and simulations, *Spec. Pap. Geol. Soc. Am.*, *186*, 101–121, 1981.

Greeley, R., N. Lancaster, S. Lee, and P. Thomas, Martian Aeolian processes, sediments and features, in *Mars*, edited by H. H. Kieffer et al., pp. 730–766, Univ. of Ariz. Press, Tucson, 1992.

Greeley, R., M. Kraft, R. Sullivan, G. Wilson, N. Bridges, K. Herkenhoff, R. O. Kuzmin, M. Malin, and W. Ward, Aeolian features and processes at the Mars Pathfinder landing site, *J. Geophys. Res.*, *104*, 8573–8584, 1999.

Greeley, R., G. Wilson, R. Coquilla, B. White, and B. Haberle, Windblown dust on Mars: Laboratory simulations of flux as a function of surface roughness, *Planet. Space Sci.*, *48*, 1349–1355, 2000.

Greeley, R., J. D. Iversen, G. Beardmore, B. Mickelson, and S. M. Metzger, Martian dust devils: Laboratory simulations, *Lunar Planet. Sci.* [CD-ROM], *XXXII*, abstract 1888, 2001.

Greeley, R., N. T. Bridges, R. O. Kuzmin, and J. E. Laity, Terrestrial analogs to wind-related features at the Viking and Pathfinder landing sites on Mars, *J. Geophys. Res.*, *107*(E1), 5005, doi:10.1029/2000JE001481, 2002.

Green, S. I., *Fluid Vortices*, 879 pp., Kluwer Acad., Norwell, Mass., 1995.

Hallett, J., and T. Hoffer, Dust devil systems, *Weather*, *26*, 247–250, 1971.

Hess, G. D., and K. T. Spillane, Characteristics of dust devils in Australia, *J. Appl. Meteorol.*, *29*, 498–507, 1990.

Hsu, C. T., and B. Fattahi, Mechanism of tornado funnel formation, *Phys. Fluids*, *19*, 1853–1857, 1976.

Idso, S. B., Tornado or dust devil, the enigma of desert whirlwinds, *Am. Sci.*, *62*, 530–541, 1974.

Iversen, J. D., and B. White, Saltation threshold on Earth Mars and Venus, *Sedimentology*, *29*, 111–119, 1982.

Iversen, J. D., R. Greeley, J. B. Pollack, and B. R. White, Simulation of Martian Aeolian phenomena in the atmospheric wind tunnel, *NASA Spec. Publ.*, *NASA SP336*, *1910213*, 1973.

Iversen, J. D., R. Greeley, and J. B. Pollack, Windblown dust on Earth Mars and Venus, *J. Atmos. Sci.*, *33*, 2425–2429, 1976a.

Iversen, J. D., J. B. Pollack, R. Greeley, and B. White, Saltation threshold on Mars, the effect of interparticle force, surface roughness and low atmospheric density, *Icarus*, *9*, 382–393, 1976b.

Iversen, J. D., R. Greeley, J. B. Marshall, and J. B. Pollack, Aeolian saltation threshold: The effect of density ratio, *Sedimentology*, *34*, 699–706, 1987.

Ives, R. L., Behavior of dust devils, *Bull. Am. Meteorol. Soc.*, *28*, 168–174, 1947.

Kahn, R. A., T. Z. Martin, R. W. Zurek, and S. W. Lee, The Martian dust cycle, in *Mars*, edited by H. H. Kieffer et al., pp. 1017–1055, Univ. of Ariz. Press, Tucson, 1992.

Kaimul, J. C., and J. A. Bussinger, Case studies of a convective plume and a dust devil, *J. Appl. Meteorol.*, *9*, 612–620, 1970.

Kuzmin, R. O., and R. Greeley, Local and regional aeolian geomorphology at the Mars Pathfinder landing site area: Evidence for paleowind regime, *Lunar Planet. Sci*. [CD-ROM], *XXX*, abstract 1415, 1999.

Lugt, H. J., *Vortex Flow in Nature and Technology*, John Wiley, New York, 1983.

Malin, M. C., and K. S. Edgett, MGS MOC the first year: Geomorphic processes and landforms, *Lunar Planet. Sci*. [CD-ROM], *XXX*, abstract 1028, 1999.

Malin, M. C., and K. S. Edgett, Mars Global Surveyor Mars Orbiter Camera: Interplanetary cruise through primary mission, *J. Geophys. Res.*, *106*, 23,429–23,570, 2001.

Malin, M. C., et al., Early views of the Martian surface from the Mars Orbiter Camera of Mars Global Surveyor, *Science*, *279*, 1681–1685, 1998.

Martin, L. J., and R. W. Zurek, An analysis of the history of dust activity on Mars, *J. Geophys. Res.*, *98*, 3221–3246, 1993.

McKim, R., The dust storms of Mars, *J. Br. Astron. Assoc.*, *106*, 185–200, 1995.

Metzger, S. M., Dust devils as aeolian transport mechanisms in southern Nevada and in the Mars Pathfinder landing site, Ph.D. thesis, Univ. of Nev., Reno, 1999.

Metzger, S. M., Recent advances in understanding dust devil processes and sediment flux on Earth and Mars, *Lunar Planet. Sci.* [CD-ROM], *XXXII*, abstract 2157, 2001.

Metzger, S. M., and N. Lancaster, Dust devil activity in a playa basin, southern Nevada, *Eos Trans. AGU*, *76* (46), Fall Meet. Suppl., F66, 1995.

Metzger, S. M., J. R. Carr, J. R. Johnson, M. Lemmon, and T. J. Parker, Dust devil vortices identified in the Mars Pathfinder camera images (abstract), *Bull. Am. Astron. Soc.*, *30*, 1023, 1998a.

Metzger, S. M., J. R. Carr, J. R. Johnson, M. Lemmon, and T. J. Parker, Dust devil vortices identified in the Mars Pathfinder camera images-Exploring the land-atmosphere link, *Eos Trans. AGU*, *79*, F537, Fall Meet. Suppl., 1998b.

Metzger, S. M., J. R. Johnson, J. R. Carr, T. J. Parker, and M. Lemmon, Dust devil vortices seen by the Mars Pathfinder Camera, *Geophys. Res. Lett.*, *26*, 2781–2784, 1999.

Metzger, S. M., J. R. Carr, J. R. Johnson, T. J. Parker, and M. Lemmon, Techniques for identifying dust devils in Mars Pathfinder images, *IEEE Trans. Geosci. Remote*, *38*, 870–876, 2000.

Neubauer, F. M., Thermal convection in the Martian atmosphere, *J. Geophys. Res.*, *71*, 2419–2426, 1966.

Pollack, J. B., D. S. Colburn, F. M. Flasar, R. Kahn, C. E. Carlston, and D. Pidek, Properties and effects of dust particles suspended in the Martian atmosphere, *J. Geophys. Res.*, *84*, 2929–2945, 1979.

Pollack, J. B., M. E. Ockert-Bell, and M. K. Shepard, Viking lander image analysis of Martian atmospheric dust, *J. Geophys. Res.*, *100*, 5235–5250, 1995.

Renno, N. O., A. A. Nash, J. Lunine, and J. Murphy, Martian and terrestrial dust devils: Test of a scaling theory using Pathfinder data, *J. Geophys. Res.*, *105*(E1), 1859–1865, 2000.

Ringrose, T. J., and J. C. Zarnecki, Martian and terrestrial dust devils, *Lunar Planet. Sci.* [CD-ROM], *XXXIII*, abstract 1183, 2002.

Rossi, A. P., Possible dust devils tracks detected in Tenere Desert, (Niger): An analogue to Mars, *Lunar Planet. Sci.* [CD-ROM], *XXXIII*, abstract 1307, 2002.

Ryan, J. A., and J. J. Carroll, Dust devils wind velocities: Mature state, *J. Geophys. Res.*, *75*, 531–541, 1970.

Ryan, J. A., and R. D. Luchich, Possible dust devil vortices on Mars, *J. Geophys. Res.*, *88*, 11,005–11,011, 1983.

Sagan, C., and J. B. Pollack, Windblown dust on Mars, *Nature*, *223*, 791–794, 1969.

Sagan, C., J. Veverka, and P. Gierasch, Observational consequences of Martian wind regions, *Icarus*, *22*, 24–47, 1971.

Schiewsow, R. L., and R. E. Cupp, Remote Doppler velocity measurements of atmospheric dust devil vortices, *J. Appl. Opt.*, *15*, 1–2, 1975.

Schofield, J. T., J. R. Barnes, D. Crisp, R. M. Haberle, S. Larsen, J. A. Magalhães, J. R. Murphy, A. Seiff, and G. Wilson, The Mars Pathfinder atmospheric structure investigation/meteorology (ASI/MET) experiment, *Science*, *278*, 1752–1758, 1997.

Seiff, A., et al., The atmospheric and meteorology instrument on the Mars Pathfinder Lander, *J. Geophys. Res.*, *102*(E2), 4045–4056, 1997.

Sinclair, P. C., A quantitative analysis of the dust devil, Ph.D. thesis, Univ. of Ariz., Tucson, 1966.

Sinclair, P. C., General characteristics of dust devils, *J. Appl. Meteorol.*, *8*, 32–45, 1969.

Sinclair, P. C., The lower structure of dust devils, *J. Atmos. Sci.*, *30*, 1599–1619, 1973.

Smith, P. H., Results from the Mars Pathfinder camera, *Science*, *278*, 1758–1765, 1997.

Smith, P. H., and M. T. Lemmon, Opacity of the Martian atmosphere measured by the Imager for Mars Pathfinder, *J. Geophys. Res.*, *104*, 8975–8985, 1999.

Tanner, W. F., Spiral flow in rivers, shallow seas, dust devils and models, *Science*, *139*, 41–42, 1963.

Thomas, P., and P. J. Gierasch, Dust devils on Mars, *Science*, *230*, 175–177, 1985.

Thomas, P. C., M. C. Malin, M. H. Carr, G. E. Danielson, M. E. Davies, W. K. Hartmann, A. P. Ingersoll, P. B. James, A. S. McEwen, L. A. Soderblom, and J. Veverka, Bright dunes on Mars, *Nature*, *397*, 592–594, 1999.

Tomasko, M. G., L. R. Doose, M. Lemmon, P. H. Smith, and E. Wegryn, Properties of dust in the Martian atmosphere from the image on Mars Pathfinder, *J. Geophys. Res*, *104*, 8987–9007, 1999.

Tratt, D. M., M. H. Hecht, D. C. Catling, and E. C. Samulon, In situ measurements of dust devil dynamics, *Eos Trans. AGU*, *82*(*47*), Fall Meet. Suppl., abstract P31A-0539, 2001.

Wells, G. L., and J. R. Zimbelman, Extraterrestrial arid surface processes, in *Arid Zone Geomorphology: Processes, Form and Change*, edited by D. S. Thomas, pp. 335–358, Halsted, New York, 1989.

White, B. R., B. M. Lacchia, R. Greeley, and R. N. Leech, Aeolian behavior of dust in a simulated Martian atmosphere, *J. Geophys. Res.*, *102*, 25,629–25,640, 1997.

Zurek, R. W., J. R. Barnes, R. M. Haberle, J. B. Pollack, J. E. Tillman, and C. B. Leovy, Dynamics of the atmosphere of Mars, in *Mars*, edited by H. H. Kieffer et al., pp. 799–817, Univ. of Ariz. Press, Tucson, 1992.

M. R. Balme and R. Greeley, Department of Geological Sciences, Arizona State University, Box 871404, Tempe, AZ 85287-1404, USA. (greeley@asu.edu)

J. D. Iversen, Aerospace Engineering and Engineering Mechanics Department, Iowa State University, Ames, IA 50011-2271, USA.

S. Metzger, Department of Geological Sciences, University of Nevada at Reno, Mail Stop 172, Reno, NV 89557, USA.

R. Mickelson,1821 West Seldon Way, Phoenix, AZ 85201, USA.

J. Phoreman, NASA Ames Research Center, Mail Stop 242-6, Moffett Field, CA 94035-1000, USA.

B. White, Department of Mechanical and Aerospace Engineering, University of California at Davis, Davis, CA 95616-5294, USA.